Journal of Industrial and Management Optimization

https://www.aimspress.com/journal/jimo

JIMO, 22(4): 1758–1788.
DOI:10.3934/jimo.2026065
Received: 23 October 2025
Revised: 31 January 2026
Accepted: 25 February 2026
Published: 11 March 2026

Research article

An adaptive PSO-based framework for energy storage efficiency and reliability maximization in wind power grid integration

Chia-Hung Wang[1,2,*], Hongzhen Yan[1], Haitao Liu[3], Qigen Zhao[4] and Xiaojing Wu[5]

[1] College of Computer Science and Mathematics, Fujian University of Technology, Fujian 350118, China

[2] Fujian Provincial Key Laboratory of Big Data Mining and Applications, Fujian 350118, China

[3] School of Big Data, Fuzhou University of International Studies and Trade, Fujian 350202, China

[4] Shenzhen Megmeet Electrical Co.,Ltd, Guangdong 518057, China

[5] College of Electronics, Electrical Engineering and Physics, Fujian University of Technology, Fujian 350118, China

* **Correspondence:** Email: 61201506@fjut.edu.cn.

Abstract: In wind power, energy storage systems (ESSs) are widely used to address power fluctuations and grid connection risks. However, optimizing the configuration of these systems presents a significant challenge. This paper introduces a novel approach, namely the adaptive particle swarm optimization (APSO), which offers several key advancements. First, it introduces a novel linear inertia weight mechanism based on the sine function, which dynamically adjusts the search behavior of particles across different optimization stages. Second, it incorporates a hybrid update strategy that integrates Levy flight, quasi-opposition-based learning, and global best guidance, enabling the algorithm to adaptively switch among different search modes. Third, an immigration operator is designed to facilitate information exchange between two subpopulations, enhancing thr search diversity and preventing premature convergence. Additionally, the algorithm is applied to both the optimal configuration and scheduling models of ESSs, demonstrating its effectiveness in reducing the system's costs, stabilizing wind power output, and mitigating grid connection risks. The proposed APSO is validated against several established algorithms using a comprehensive test suite comprising 92 benchmarks, showing competitive or superior performance in most cases and confirming its practical value in ESS optimization.

Keywords: adaptive particle swarm optimization; energy storage system; optimal configuration; wind power integration; wind power generation
Mathematics Subject Classification: 68T05, 90C26

1. Introduction

According to the presence or absence of energy storage devices, smooth power output schemes are mainly divided into two categories, namely, smooth power output schemes containing energy storage devices and smooth power output schemes without energy storage devices [1]. A smooth power output scheme without energy storage equipment mainly relies on the adjustment ability of the equipment itself for smoothing power, which is relatively limited, and the addition of energy storage equipment will greatly improve the ability to output power smoothly [2]. In the past, the development of energy storage in China has mainly concentrated on pumped storage energy, whereas in recent years, attention to all kinds of energy storage equipment has gradually increased. At the national level, many polices have been officially released, proposing that the market trading mechanism and price mechanism of energy storage should be improved, indicating that policies for energy storage should be established and that power companies that configure their energy storage facilities should be helped to participate in the auxiliary service market and the power spot market [3]. Energy storage devices such as battery energy storage systems (BESSs) [4], have several advantages, such as high efficiency, fast response, low maintenance, compact size and ease of installation. Therefore, a BESS is the most commonly used ESS to smooth wind power output [5]. Figure 1 shows the structure of the system used in this paper, which helps us obtain a better understanding of the role of the ESS and its place in the overall system. Meanwhile, with the depletion of conventional energy sources, there is a growing need to transition towards clean energy sources.

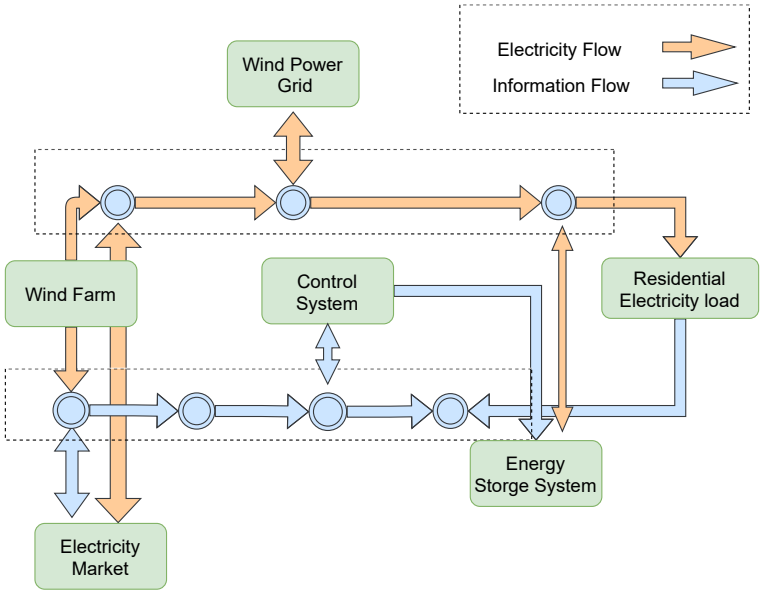

Figure 1. The structure of the overall system containing an ESSs.

Wind power has emerged as a prominent renewable energy option [6]. However, wind power generation's intermittent and unpredictable nature leads to significant fluctuations linked to wind speed. The power produced by wind turbines can vary widely due to changes in wind speed, causing fluctuations that complicate the grid's stability [7]. This introduces significant challenges for ESSs in terms of both storage capacity and discharge capabilities. Energy storage devices must efficiently absorb the excess power generated during high wind periods and release it when wind power generation is low, thereby

ensuring that the grid maintains a stable supply of power [8]. However, this process requires a highly responsive ESSs that is capable of handling the rapid fluctuations in wind generation. Another challenge lies in the degradation of ESSs' performance over time, particularly in BESSs, where the repeated charge and discharge cycles can reduce the system's efficiency and lifespan [9]. The optimal sizing and placement of ESSs within wind power systems are also crucial for minimizing these degradation effects while ensuring that energy storage can effectively smooth out wind power fluctuations. Furthermore, energy losses during energy storage and discharge cycles can reduce the overall efficiency of the system, making it more difficult to achieve cost-effective integration of wind power.

These fluctuations pose challenges to the stability of power grid operations and result in harmonic pollution [10, 11]. To ensure the safety and reliability of power grid operations, various methods and strategies for ESSs have been proposed in many studies to address the challenges posed by wind power fluctuations and its integration.

For instance, a control strategy was proposed to reduce wind power fluctuations using a battery-supercapacitor hybrid energy storage system (HESS) [12]. This approach utilizes self-adaptive wavelet packet decomposition technology and a two-stage method for distributing power reference signals. A new robust dynamic-wavelet-enabled approach was designed for wind power smoothing by utilizing the HESS [13]. This approach effectively addresses wind power's uncertainty.

The improved sailfish algorithm was used to address the economic scheduling problem of power system and achieve lower operation costs [14]. The algorithm and some similar applications [15, 16] imply the possibility of applying the optimization algorithm so the optimal configuration of ESSs can be explored. The lightning search algorithm (LSA) [17] was used for the installation of wind power generation models [18] and the optimization of radial distribution networks with multiple distributed generators (DGs) and distributed static synchronous compensators (DSTATCOMs) [19]. Heuristic algorithms are commonly used to solve the optimal configuration problem of energy storage systems, which involves selecting the appropriate storage capacity, type, and location while ensuring the system's stability. For instance, the particle swarm optimization (PSO) algorithm has been applied in wind power systems to determine the optimal storage capacity and the placement of storage devices, thereby enhancing the system's ability to regulate wind power fluctuations and reducing costs [20]. By continuously optimizing the parameters, PSO can effectively find the optimal solution for energy storage systems' configuration. Therefore, we focus on PSO, one of the most well-known optimization algorithms.

PSO, first introduced in 1995 by Kennedy et al. [21], is a nature-inspired evolutionary algorithm. PSO conceptualizes each candidate solution to an optimization problem as a bird or particle. The group of particles, also known as a swarm, navigates the D-dimensional search space inherent to the problem. The position of a particle is influenced by both its individual experiences and those of its neighboring particles. The insufficient use of population information has exhibited several drawbacks, impacting not only scientific research but also various engineering applications [22]. Therefore, a variant of PSO that called the comprehensive learning particle swarm optimizer (CLPSO) [23] was proposed. This method uses an innovative learning strategy in which the historical best information of all other particles is utilized to update the velocity of a given particle. Nasir et al. [24] further extended the CLPSO algorithm by delimiting the exemplar particle to a dynamic neighborhood. Another dynamic neighborhood-based switching PSO (DNSPSO) [25] algorithm was also proposed. In this approach, a novel velocity updating mechanism is crafted to adapt the personal best position and the global best

position based on a distance-dependent dynamic neighborhood. This is devised to fully leverage the population evolution information within the entire swarm.

At the same time, the fixed parameters of c_1 and c_2 and inertia weights of canonical PSO cannot be adjusted with the population update. Therefore, besides exploiting the information within the population, PSO researchers also proposed parameter-based techniques for performance improvements [26, 27]. Shi and Eberhart [28] observed that introducing an inertia weight in the velocity component of the PSO algorithm generally accelerates convergence. Therefore, the iteration equation incorporating an inertia weight was adopted in subsequent PSO variants. Taherkhani and Safabakhsh [29] introduced a PSO variant where the inertia weight for each dimension of a particle varied, with its values determined by the performance of the particle and the distance from its historical best position. A chaos-based nonlinear inertia weight called modified particle swarm optimization (MPSO) was proposed by Liu et al. [30]. A PSO variant was proposed by Meng et al. called PSO-sono [31] for single-objective optimization, which included novel adaption schemes for the ratio of each paradigm, and constriction coefficients are proposed during each iteration.

In addition to the aforementioned studies, numerous related works have also explored optimization-based strategies and advanced control frameworks for improving the performance of ESSs and wind power integration. For instance, model predictive control (MPC) methods [32] have been adopted to enhance dynamic performance and reduce ramping fluctuations in wind power systems, while multiobjective optimization frameworks have been used to simultaneously address systems' cost, stability, and reliability. Furthermore, several PSO extensions—such as multi-swarm PSO [33], quantum-behaved PSO [34], and hybrid PSO–GA [20] have been used for renewable energy scheduling, ESS sizing, and grid-support service optimization, demonstrating the increasing importance of intelligent optimization in complex power system applications. These additional advancements highlight the strong potential of combining ESS technology with enhanced swarm intelligence algorithms. Motivated by these findings, this paper further develops an improved PSO method. Specifically, the adaptive PSO (APSO) incorporates a linear inertia-weight adjustment mechanism, hybrid iterative paradigms, and dynamic weighting strategies to balance exploration and exploitation more effectively and to utilize the population information more comprehensively. This design aims to achieve better optimization performance and to improve the ESS's configuration efficiency.

In summary, PSO has the potential to enhance its performance in addressing single-objective optimization problems through three key strategies. First, by adopting a new update iterative paradigm containing different strategies , the algorithm can effectively leverage the population's information. Second, improvements can be made to the coefficients of the iterative paradigm, incorporating adaptive schemes for enhanced performance. Lastly, refining the overall algorithm framework and strategies used at different stages can contribute to improved efficiency.

In this paper, we propose a PSO variant called APSO featuring a linear inertia weight scheme and hybrid paradigms for optimizing the configuration of an ESS. The key highlights of the algorithm include the following.

1. Introduction of a sine-based linear inertia weight update scheme, dynamically adjusting the search step and search speed of particles during iteration updates. This mitigates premature convergence, ensuring a balance between exploration and exploitation.

2. Proposal of a hybrid update paradigm that integrates multiple strategies, including Levy flight for global exploration, global best guidance for directed search, and quasi-opposition-based learning

for local refinement. This allows the algorithm to adapt its search behavior on the basis of the current optimization state.

3. Implementation of a dual-subpopulation framework with an immigration operator, which promotes information sharing and enhances the population's diversity. This mechanism helps the algorithm escape local optima and makes more effective use of population information.

4. Application of the algorithm to the optimal configuration of an ESS, resulting in cost reduction, stabilization of wind power, and a decreased wind power grid connection risks.

5. Performance verification experiments involve testing the algorithm on four test suites for real parameter single-objective optimization, including a test suite of 23 classic benchmarks [35], and the CEC2013 [36], CEC2017 [37], and CEC2022 test suites [38].

The subsequent sections of the paper are organized as follows. In Section 2, we provide a brief review of several PSO variants and contrasting algorithms relevant to this study and the model of the optimal configuration and optimal scheduling of the ESS. In Section 3, we introduce the framework and details of the proposed APSO algorithm. In Section 4, we validate the algorithm's performance on various test suites and apply it to optimize the configuration of the ESS. Finally, our conclusions are summarized in Section 5.

2. Related works

In this section, this paper provides a comprehensive overview of the optimal configuration and optimal scheduling of the ESSs, including their mathematical models. Several closely related PSO variants, including the modified PSO with chaotic-based inertia weight (MPSO), the comprehensive learning PSO (CLPSO), and the snake optimizer (SO) [39], will be reviewed.

2.1. Optimizing the configuration of the ESS

At present, the mainstream energy storage configuration methods can be divided into the configuration method based on sequential operation simulation, the deterministic configuration method, and the uncertain configuration method [40]. The deterministic configuration method [41] takes the rated power and rated capacity of the ESS as the decision variables of the model, based on the deterministic assumption of data samples combined with the historical operating data of the system, and establishes a renewable ESS model that optimizes the energy storage configuration considering economy or technology. Then a suitable solution algorithm is adopted to get the optimal configuration result for energy storage.

The operational efficacy and economic benefits of an optimally configured ESS are fundamentally dependent on the precise management of its core component, the battery. Advanced algorithms for real-time state estimation, such as the state of charge (SOC) and state of power (SOP), are crucial in this context. Recent research has focused on enhancing the accuracy and robustness of these estimations under varying conditions. For instance, Wang et al. developed a square root-untraced Kalman filtering strategy with full-parameter online identification for the joint evaluation of the SOC and SOP [42]. Another study introduced an improved multifeature electrochemical thermal coupling model for reliable SOC prediction at low temperatures [43], while a separate approach utilized a PSO with an adaptive square root cubature Kalman filter to achieve high-precision SOC estimation [44]. The high-fidelity state information provided by such methods is indispensable for implementing the effective scheduling strategies discussed subsequently.

In the electricity market, wind power forecasting and energy storage scheduling strategies play crucial roles in transactions involving power sales and purchases [45]. Wind power forecasting assists wind power systems in better understanding future wind energy production, enabling the formulation of rational strategies for buying and selling electricity. On the other hand, energy storage scheduling strategies help ESSs more effectively manage energy storage and release, facilitating more balanced supply and demand, reducing costs, and enhancing efficiency [46].

Researchers have made many attempts to deal with the wind power output problem succinctly and efficiently in the optimal scheduling model. These can be divided into deterministic models, probabilistic models, fuzzy models, and so on [41]. Deterministic models use deterministic methods, such as simulation models based on physical models. The model uses mathematical formulas to build a physical model of the wind turbine, describing its physical behavior and using the known conditions to predict the power output of the wind turbine.

Many researchers have made novel contributions to the optimal configuration and scheduling of ESSs, and some important studies are summarized in Table 1.

Table 1. Related works about optimizing the configuration of wind power ESSs.

Literature	System	Optimizer	Purpose	Contribution
[47]	HESS	×	Smooth fluctuations	EEMD
[48]	DBESS	×	Smooth fluctuations	DBESS
[13]	HESS	×	Smooth fluctuations	Robust dynamic wavelet-enabled approach
[12]	HESS	×	Smooth fluctuations	Novel control strategy
[49]	HESS	×	Smooth fluctuations	A probabilistic approach
[50]	HESS	×	Smooth fluctuations	Novel configuration algorithm
[51]	BESS	×	Smooth fluctuations	Novel control strategy
Our work	BESS	APSO	Smooth fluctuations	APSO

2.2. The model of optimal configuration of an ESS for mitigating wind power fluctuations

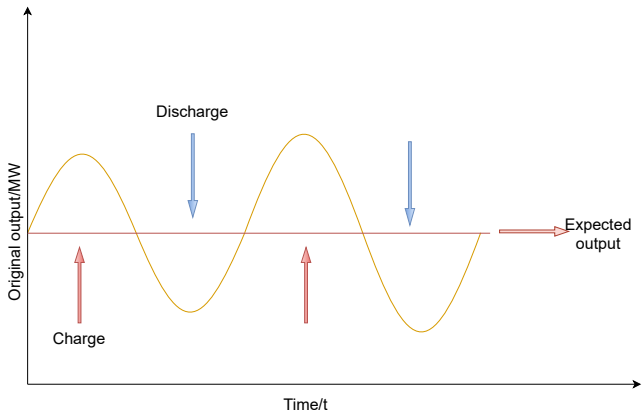

Figure 2. Brief schematic diagram of the principle for mitigating fluctuation.

As shown in Figure 2, the ESS is charged when the original output power is greater than the desired output; otherwise, it is discharged. This strategy aims to address the inherent variability in wind power generation, ultimately enhancing its reliability and stability [52]. This section comprehensively

considers the revenue of reducing wind curtailment after configuring energy storage, the penalties for mitigating insufficiency, and the costs associated with adding ESSs. The objective function is formulated to minimize the total cost of the ESS, with the optimal energy storage capacity determined as the one that achieves this minimum cost.

2.2.1. Objective function

$$\min F = C_{inv} + C_{om} + C_{lack} + C_{abandon} + C_{rec}, \tag{2.1}$$

where we have the initial investment cost C_{inv} , the operational cost C_{om} , and the penalty for insufficient suppression C_{lack} . Additionally, the symbol $C_{abandon}$ signifies the cost associated with wind power curtailment, while C_{rec} represents the full lifecycle cost of the battery used in the ESS. The calculation of the initial investment cost is as follows:

$$C_{inv} = C_E C_{ES} + C_P P_{ES}, \tag{2.2}$$

where the notations C_{ES} and P_{ES} represent the rated capacity and rated power of the ESS, respectively. The unit capacity and unit power costs of the ESS are denoted as C_E and C_P .

The lifecycle cost of the battery used in the ESS is calculated by using the rainflow counting method [53]. This involves assuming a maximum cycle count of $N_{bess,\max}$ and a depth of discharge x . The battery's cycle count and depth of discharge characteristics are determined by its external specifications. The battery's lifecycle is closely related to its operating conditions. The deeper the depth of discharge x , the shorter the cycling life. The equivalent cycle count for the battery is defined as

$$\omega(x) = \frac{N_{bess,\max}}{N_{Bess}(x)}. \tag{2.3}$$

Here, the cycle count of the battery at a depth of discharge x is denoted as $N_{Bess}(x)$, and the notation $\omega(x)$ signifies the equivalent number of cycles for the battery at a depth of discharge x , assuming that it is equivalent to the number of cycles under full charge discharge conditions.

Assuming that the battery undergoes m charge–discharge cycles per day, with each cycle having a depth of discharge x_j , $j = 1, 2, \cdots, m$. The equivalent cycle count for the battery can be calculated as follows:

$$N_D = \sum_{j=1}^{m} \omega(x_j). \tag{2.4}$$

Therefore, the operational lifespan of the battery $T_{BESS} = {}^{N_{bess,\max}}\!/_{365N_D}$, measured in years. The cycle count at the depth of discharge $N_{Bess}(x)$ is given by

$$N_{Bess}(x) = a_1 + a_2 e^{a_3 x} + a_4 e^{a_5 x}, \tag{2.5}$$

where the symbols a_1 to a_5 are determined by the battery's own parameters. Given the cycling life of a specific model of lead–acid battery at different depths of discharge [54], we performed curve fitting based on the data in the paper and obtained the values for a_1 to a_5 . The number of ESS replacements during the project's lifespan ε is given by

$$\varepsilon = \frac{T}{T_{BESS}}, \tag{2.6}$$

where the project's lifespan is denoted as T . The lifecycle cost of the battery can be expressed using the following formula:

$$C_{rec} = (k_{pr}P_{HN} + k_{er}E_{HN})(\varepsilon + 1)(1 + r)^{-T}, \tag{2.7}$$

where the notations k_{pr} and k_{er} are the unit power handling cost and unit capacity handling cost, respectively. Additionally, P_{HN} and E_{HN} denote wind power and the ESS's capacity.

The operation and maintenance costs of an ESS refer to the expenses required to maintain the system's normal operation. These include the costs for equipment maintenance, monitoring, and control, as well as management and insurance fees. When C_{om} is difficult to determine, it is typically approximated on the basis of a certain percentage of the initial investment.

$$C_{om} = P_{ES}C_{omp} + C_{ES}C_{ome}, \tag{2.8}$$

where the symbols C_{omp} and C_{ome} represent the unit power and unit capacity operation and maintenance costs of the ESS. Accounting for the time value of money, the economic cost of the ESS is converted into an equivalent annual cost C, calculated as follows:

$$C = \frac{d_r(d_r + 1)^T}{(d_r + 1)^T - 1}(C_{inv} + C_{om}), \tag{2.9}$$

where d_r represents the discount rate, and T is the system's lifespan. Meanwhile, the fraction $d_r(d_r + 1)^T \big/ (d_r + 1)^T - 1$ is the capital recovery factor. The penalties for mitigating insufficiency and wind power curtailment costs are given by

$$C_{\text{lack}} + C_{abandon} = \alpha E_{lack} + \beta E_{abandon}, \tag{2.10}$$

where the notations α and β represent the unit penalty costs for mitigating insufficiency and wind curtailment. In Equation (2.10), the symbols E_{lack} and $E_{abandon}$ are the annual quantities of mitigating insufficiency and wind curtailment.

Taking into account the economic cost of the ESS, the penalty for mitigating insufficiency, and the penalty for wind power curtailment, the objective function for the optimization of the ESS configuration is given by

$$\min F = C + \alpha E_{lack} + \beta E_{abandon} + C_{rec}. \tag{2.11}$$

2.2.2. Constraints

To ensure compliance with national grid standards for wind power, this paper uses a sliding average filter to determine the expected wind power output, denoted $P_R(t)$ and expressed as

$$P_R(t) = \frac{1}{T}\sum_{k=t-(\frac{T}{2}-1)}^{t+\frac{T}{2}} R(k), \tag{2.12}$$

where the original wind power output at time k is denoted by $R(k)$. At time t , the expected wind power output is denoted as $P_R(t)$. The symbol T represents the length of the sliding average window. By choosing an appropriate value for T, wind power output can be effectively smoothed while ensuring compliance with national grid standards, avoiding excessive or insufficient smoothing. In this section,

the ESS's capacity for limiting wind power fluctuations is expressed as a constraint, where the wind power fluctuations under any different sliding average window during the operational cycle should not exceed 15%. The charging and discharging output capabilities of the ESS are given by the following formulas:

$$P_c(t) = \min\left\{\bar{P}_c, \frac{B - S(t)}{\eta \Delta t}, \max\{0, R(t) - D(t)\}\right\}, \tag{2.13}$$

$$P_d(t) = \min\left\{\bar{P}_d, \frac{S(t)\beta}{\Delta t}, \max\{0, D(t) - R(t)\}\right\}, \tag{2.14}$$

where the wind power generation at time t is denoted as $R(t)$, the load power at time t is denoted as $D(t)$, and the notation $S(t)$ represents the state of charge at time t . Additionally, $\max\{0, R(t) - P_r(t)\}$ represents the charging demand of the ESS when there is a power surplus. Meanwhile, the maximum charging power is denoted as $\bar{P}_c$, the notation B is the maximum capacity of the ESS, and η is the charging efficiency. The maximum charging power is denoted as $^{B - S(t)}/_{\eta \Delta t}$ to ensure that the ESS does not exceed its maximum capacity during the charging period.

Similarly, the notation $\max\{0, P_r(t) - R(t)\}$ represents the discharge demand of the ESS during power shortage, the maximum discharge power is denoted as $\bar{P}_d$. The discharge efficiency of the ESS is represented by β , while the notation $^{S(t)\beta}/_{\Delta t}$ ensures that the ESS does not fall below the minimum capacity during discharge.

Since the charging and discharging processes of the ESS cannot occur simultaneously, the model satisfies the following equation:

$$P_d(t) \cdot P_c(t) = 0. \tag{2.15}$$

The SOC of the ESS is calculated as follows:

$$S(t+1) = \eta P_c(t) \Delta t - \frac{P_d(t)}{\beta} \Delta t + S(t), \tag{2.16}$$

where the notation $S(t)$ represents the SOC at time t . Additionally, the SOC of the system is subject to constraints on the state of charge of the ESS.

$$SOC_{\max} \geq S(t) \geq SOC_{\min}, \tag{2.17}$$

where the upper and lower limits of the SOC of the energy storage battery are denoted as $SOC_{\max}$ and $SOC_{\min}$, respectively.

Given this description, the optimization problem for configuring the ESS to mitigate wind power fluctuations can be formulated as follows.

Minimize

$$F = C + \alpha E_{lack} + \beta E_{abandon} + C_{rec}, \tag{2.18}$$

subject to

$$P_R(t) = \frac{1}{T} \sum_{k=t-(\frac{T}{2}-1)}^{t+\frac{T}{2}} R(k), \tag{2.19}$$

$$P_c(t) = \min\left\{\bar{P}_c, \frac{B - S(t)}{\eta \Delta t}, \max\{0, R(t) - D(t)\}\right\}, \tag{2.20}$$

$$P_d(t) = \min\left\{\bar{P}_d, \frac{S(t)\beta}{\Delta t}, \max\{0, D(t) - R(t)\}\right\}, \tag{2.21}$$

$$P_d(t) \cdot P_c(t) = 0, \tag{2.22}$$

$$S(t+1) = \eta P_c(t)\Delta t - \frac{P_d(t)}{\beta}\Delta t + S(t), \tag{2.23}$$

$$SOC_{\max} \geq S(t) \geq SOC_{\min}. \tag{2.24}$$

where

$$C = \frac{d_r(d_r+1)^T}{(d_r+1)^T - 1}(C_{inv} + C_{om}), \tag{2.25}$$

$$\alpha E_{lack} + \beta E_{abandon} = C_{\text{lack}} + C_{abandon}, \tag{2.26}$$

$$C_{rec} = (k_{pr}P_{HN} + k_{er}E_{HN})(\varepsilon + 1)(1+r)^{-T}. \tag{2.27}$$

2.3. The model of optimal scheduling of the ESS combined with short-term power predictions

The core idea of establishing an energy storage optimization system considering wind power forecasting and power purchase agreement mechanisms in this section is to minimize the total cost over the planning period. This is achieved by optimizing the charging and discharging operations of the ESS during appropriate time periods. Additionally, through optimal energy control strategies that involve buying and selling electricity in the electricity market, the system aims to enhance the operator's revenue and maximize the utilization of wind energy resources.

2.3.1. Objective function

In the studied optimization model, we have the following objective function:

$$\min F = C - C_{revenue}, \tag{2.28}$$

where the symbol

$$C = \frac{d_r(d_r+1)^Y}{(d_r+1)^Y - 1}(C_{inv} + C_{om}), \tag{2.29}$$

is the total energy storage cost, C_{inv} and C_{om} are the initial investment cost and operational cost, respectively. Meanwhile, in the objective function in Equation (2.28), the parameter $C_{revenue}$ is

$$C_{revenue} = \sum_{t=1}^{T} P_{sale}(t) \times p_{sale}(t) - \sum_{t=1}^{T} P_{purchase}(t) \times p_{purchase}(t), \tag{2.30}$$

where the symbol d_r represents the discount rate, and Y is the system's lifespan. In Equation (2.29), the fraction $d_r(d_r+1)^Y \big/ (d_r+1)^Y - 1$ is the capital recovery factor. Moreover, $C_{revenue}$ represents the total revenue from buying and selling electricity in the power market throughout the year. The symbol $P_{sale}(t)$ is the amount of electricity sold to the power market at time t, and $P_{purchase}(t)$ is the amount of electricity bought from the power market at time. Meanwhile, $p_{sale}(t)$ and $p_{purchase}(t)$ are the selling and buying prices of electricity, respectively, at time t.

2.3.2. Constraints

The constraint conditions for the ESS are similar to those in last section. The difference lies in the expectation that the output in this section corresponds to the actual load demand. The charging and discharging output capabilities of the ESS are defined by the following formulas:

$$P_c(t) = \min\left\{\bar{P}_c, \frac{B - S(t)}{\eta\Delta t}, \max\{0, R(t) - D(t)\}\right\}, \tag{2.31}$$

$$P_d(t) = \min\left\{\bar{P}_d, \frac{S(t)\beta}{\Delta t}, \max\{0, D(t) - R(t)\}\right\}. \tag{2.32}$$

Here, the generated power of the wind farm at time t is given by $R(t)$, and the power demand at time t is denoted as $D(t)$.

2.3.3. Indicators

In our model, the reliability of the system is measured through the loss of power supply expectation (LOPSE), which is the expected quantity of energy shortage compared with $D(t)$, which is calculated as follows:

$$LOPSE = \frac{1}{T}\sum_{t=1}^{T} \max\{(D(t) - P_{out}(t)), 0\}, \tag{2.33}$$

where the symbol $P_{out}(t)$ represents the final output of the ESS at time t. The renewable energy utilization rate is determined by the following formula:

$$U_{RG} = \frac{\sum_{t=1}^{T} \min\{D(t), P_{out}(t)\}\Delta t}{\sum_{t=1}^{T} R(t)\Delta t}. \tag{2.34}$$

2.3.4. Two-stage scheduling strategy

Under an appropriate energy storage configuration, the wind power ESS ensures the smoothness of its output, avoiding curtailment caused by wind energy uncertainties. However, such an operational strategy comes with higher economic costs. When interacting with the electricity market, the economic advantages of the ESS are not fully realized. Therefore, this paper proposes an energy control strategy that considers wind power predictions and power purchase agreements to balance the economic efficiency of the ESS with the stability of wind power. The wind power prediction model used here is a short-term wind power prediction model based on an improved Markov model proposed by Wang et al. [55].

The wind power energy storage system operates in two stages: The scheduling stage and the adjustment stage. In the scheduling stage, depending on the differences in wind power and load demand, varying electricity prices, and different energy storage states, the control of the ESS is divided into four modes.

When the energy storage state is $60\%\ SOC \geq S(t) \geq 40\%\ SOC$, indicating a balanced energy surplus, the system operates in Mode One, balancing the charging and discharging to meet the load demand.

When the energy storage state is $S(t) > 60\%\ SOC$, indicating an adequate energy surplus, the system operates in Mode Two. In this mode, regardless of whether the wind power exceeds the load power in

the predicted adjustment period, if the electricity price is higher than the average, the system operates in Mode Two. If the electricity price is lower than the average, the system operates in Mode One.

On the other hand, when $S(t) < 40\%\ SOC$, indicating an insufficient energy surplus, the system operates as follows.

If the wind power exceeds the load power in the predicted adjustment period, the system operates in Mode One. If the wind power is less than the load power, and the electricity price is less than the average, the system operates in Mode Three; otherwise, it operates in Mode One.

Mode One

When the actual wind power is greater than the load power, the energy storage charges to absorb excess wind power. When the load power is greater than the wind power, the energy storage discharges to supplement the shortfall in wind power. If the storage exceeds its limit, transactions with the electricity market for selling or buying are conducted, based on surplus or deficit conditions. The entire adjustment period stays within the constraint conditions.

Mode Two

Regardless of whether the actual wind power is greater than the load power, electricity sales occur. If wind power is greater than the load power, surplus wind power and stored energy are sold until the storage state drops below 40%. If the actual wind power is less than the load power, the ESS discharges to supplement it, and stored energy is sold until the storage state drops below 40%. The entire adjustment period stays within the constraint conditions.

Mode Three

When the actual wind power is greater than the load power, the energy storage charges to absorb excess wind power. When the actual wind power is less than the load power, and the actual electricity price is lower than the average, the system purchases electricity from the market to balance the load demand. Simultaneously, the purchased electricity charges the ESS for arbitrage.

2.4. The PSO algorithm

PSO is a popular heuristic optimization algorithm inspired by the social behavior of birds flocking or fish schooling. It is used for solving complex optimization problems by mimicking the collaborative behavior of particles in a swarm. Each particle represents a potential solution, and it moves through the search space influenced by its own experience and the experience of its neighboring particles. The iteration paradigm of the canonical PSO is presented as follows:

$$V_{i,G+1} = V_{i,G} + r_1 \cdot c_1 \cdot \left(X_{pbest_i,G} - X_{i,G}\right) + r_2 \cdot c_2 \cdot \left(X_{gbest,G} - X_{i,G}\right), \tag{2.35}$$

$$X_{i,G+1} = X_{i,G} + V_{i,G+1}, \tag{2.36}$$

where the random values r_1 and r_2 fall within in the range [0,1]. The constants c_1 and c_2 constrict the cognitive part and social part of the paradigm, respectively. The symbol $V_{i,G}$ is the velocity of $X_{i,G}$, which is a D-dimensional vector denotes the i^{th} particle of the population in the G^{th} generation. Historical best locations of the particle and the global best location of the entire population are denoted as $X_{pbest_i,G}$ and $X_{gbest,G}$, respectively.

The key idea behind the PSO is to iteratively update the velocity and position of each particle to find the optimal solution. The velocity update equation (Equation 2.35) incorporates both the particle's

previous velocity and its attraction to its personal best position ($X_{pbest_i,G}$) and the global best position ($X_{gbest,G}$) found by the entire swarm. The position update (Equation 2.36) simply adds the updated velocity to the current position of the particle. This process is repeated until a predefined stopping criterion is met, such as a set number of iterations or the convergence of the solution.

2.5. The MPSO algorithm

In MPSO, a chaos-based nonlinear inertia weight was proposed, which avoids premature convergence and a balance between exploration and exploitation. The formula for updating its adaptive weights is as follows:

$$r_{G+1} = 4r_G\left(1 - r_G\right), r\left(0\right) = rand, \tag{2.37}$$

where $r_0 \notin \{0, 0.25, 0.5, 0.75, 1\}$, and we have

$$\omega_G = r_G \cdot \omega_{\min} + \frac{(\omega_{\max} - \omega_{\min}) \cdot gen}{gen_{\max}}, \tag{2.38}$$

where $\omega_{\max} = 0.9$ and $\omega_{\min} = 0.4$. A random number generated by the logistic chaotic is given by r_G . Additionally, it uses the following update paradigm:

$$\begin{cases} V_{i,G} = \omega \cdot V_{i,G} + r_1 \cdot c_1 \cdot (X_{sb_i,G} - X_{i,G}) + r_2 \cdot c_2 \cdot (\overline{X}_{center,G} - X_{i,G}) \\ X_{i,G} = \begin{cases} \omega \cdot V_{i,G} + (1 - \omega) \cdot (V_{i,G+1}) + X_{gb,G}, p_i > rand \\ X_{i,G} + V_{i,G+1}, otherwise \end{cases} \end{cases}, \tag{2.39}$$

where $X_{sb_i,G}$ denotes the stochastic learning particle of the i^{th} individual, and $\overline{X}_{center,G}$ represents the center of the population.

2.6. The CLPSO algorithm

The algorithm known as the CLPSO, is a variant of PSO that incorporates a novel learning strategy. In this strategy, the historical best information of all other particles is utilized to update the velocity of a particle. This approach aims to preserve the diversity of the swarm, discouraging premature convergence. The velocity update equation used in the learning strategy is as follows:

$$\begin{cases} V_{i,G}^d = \omega_i \cdot V_{i,G}^d + c \cdot r_{i,G} \cdot (X_{pbest_{f_i},G}^d - X_{i,G}^d) \\ X_{i,G} = X_{i,G} + V_{i,G} \end{cases}, \tag{2.40}$$

where the symbol $X_{pbest_{f_i},G}^d$ is determined by the probability Pc_i of the i^{th} particle and ω is a weight that obeys the following linear reduction:

$$Pc_i = 0.05 + 0.45 \cdot \frac{e^{10 \cdot \frac{i-1}{ps-1}} - 1}{e^{10} - 1}, \tag{2.41}$$

$$\omega = \omega_{\max} - \frac{gen}{gen_{\max}}\left(\omega_{\max} - \omega_{\min}\right). \tag{2.42}$$

2.7. The SO algorithm

Hashim and Hussien proposed a meta-heuristic algorithm called the SO, which uses an adaptive inertia weight scheme to help iteration paradigm control the search speed and search direction, balancing exploration and exploitation. The update formulas are as follows:

$$\omega_1 = \exp\left(\frac{-gen}{gen_{\max}}\right), \tag{2.43}$$

$$\omega_2 = c_1 \cdot \exp\left(\frac{gen - gen_{\max}}{gen_{\max}}\right). \tag{2.44}$$

The linear inertia weights will be compared with the fixed individual cognitive and social cognitive parameters, divided into different update stages, and the adaptive weights are combined with different adaptive parameters to jointly control the individual update in different update stages. The update paradigm is as follows:

$$\begin{cases} V_{i,G+1} = c \cdot \omega \cdot r \cdot (X - X_{i,G}) \\ X_{i,G+1} = X_{i,G} + V_{i,G+1} \end{cases}, \tag{2.45}$$

where r represents the random values in [0,1]. Note that in Equation (2.45), the two parameters ω and X have different adaptive calculations at different stages, but the update paradigm is similar to PSO. The symbol X includes the best individual of all populations, the best individual of another subpopulation, and the common individual of another subpopulation. At the same time, the inertia weight including several methods of calculation to control different update strategies in different stages.

3. The proposed APSO algorithm

In this section, a comprehensive overview of the proposed APSO algorithm will be provided, as depicted in Figure 3. The algorithm's intricacies, covering the linear inertia weight scheme and the innovative hybrid update paradigm, will be thoroughly investigated. This aims to facilitate the algorithm in escaping local optima and achieving a balance between exploration and exploitation. Additionally, the pseudocode is presented in Algorithm 1.

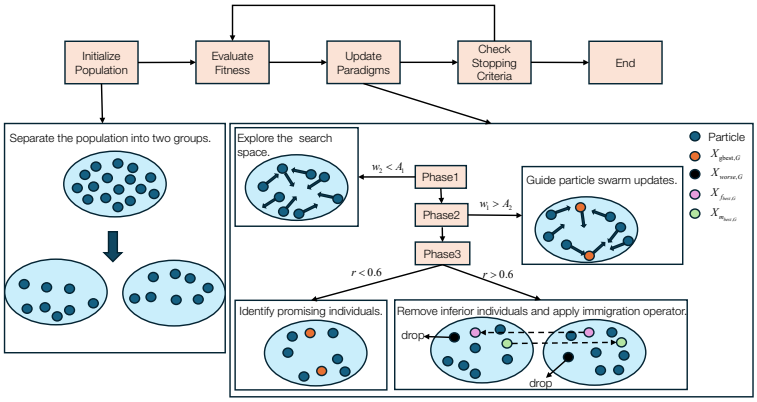

Figure 3. The novel adaptive particle swarm optimization (APSO).

Algorithm 1 Pseudocode of the proposed adaptive particle swarm optimization (APSO).

Input: Solution space $\left[X_{\min}^{D}, X_{\max}^{D}\right]$, maximum number of function evaluations $gen_{\max}$, objective function $f(X)$, population size N.
Output: Best fitness value $f(X_{gbest,G})$, optimum location $X_{gbest,G}$.
$c = 2$, $\alpha = 0.8$, $\mu = 0.01$, $A_1 = 0.25$, $A_2 = 0.6$.
Separate the population into two groups and calculate their fitness.
for $i = 1 : gen_{\max}$ **do**
    Calculate the inertia weights according to Equations (3.1) and (3.2).
    if $\omega_2 < A_1$ **then**
        Update the populations according to Equation (3.3).
    else
        if $\omega_1 > A_2$ **then**
            Update the parameter according to Equation (3.4).
            Update the populations according to Equation (3.5).
        else
            if $r < 0.6$ **then**
                Update the parameters according to Equation (3.7).
                Update the populations according to Equation (3.6).
            else
                Update the parameters according to Equation (3.9).
                Update the populations according to Equation (3.8) with the updated parameters.
                Delete the worst individuals of the subpopulations and regenerate them.
                Using the immigration operator to exchange information of the subpopulations according to Equations (3.10) and (3.11).
            end if
        end if
    end if
end for
Return: $f(X_{gbest,G})$, and $X_{gbest,G}$.

3.1. The inertia weights update schemes in the APSO

As widely recognized, setting the inertia weight is crucial for keeping the particles at a certain search velocity [56]. However, using fixed inertia weights in control may lead to an imbalance between exploration and exploitation, resulting in premature convergence [57]. To address this issue and achieve a harmonious balance between exploration and exploitation, a linear inertia weight update scheme based on the sine function is introduced [58]. This strategy enables the particles to sustain varying search speeds and directions across different search stages. For instance, at the initial stages of the algorithm, a large weight is maintained to facilitate faster exploration of the entire search space. Conversely, during later search stages, a smaller inertia weight is used to navigate the local space around promising candidate solutions, enhancing the algorithm's search precision. The update formula for the linear

inertia weights is presented below:

$$\omega_1 = \sin\left(\frac{2\pi}{gen_{\max}} \cdot gen\right), \tag{3.1}$$

$$\omega_2 = 1 - \omega_1. \tag{3.2}$$

The inertia weight controls the velocity of particles and is adaptively updated according to the optimization stage. In the initial exploration phase, a larger inertia weight is used to allow the particles to explore the search space broadly. As the algorithm progresses to later stages, the inertia weight is reduced, which allows for more focused searching around the optimal regions, thus refining the solution.

3.2. The update paradigms of the APSO

During the initial phase of the algorithm, when the particles are required to explore the entire search space, this paper constrains the stage to $\omega_2 < A_1$. During this period, inspiration was drawn from Levy's flight strategy [59], and we utilize the following update paradigm to modify the particles' position.

$$\begin{cases} V_{i,G+1} = \omega \cdot step \cdot ((X_{\max} - X_{\min}) \cdot r + X_{\min}) \\ X_{i,G+1} = X_{i,G} + V_{i,G+1} \end{cases}. \tag{3.3}$$

Here, the symbols $\omega = 0.01$ and $step$ represent the inertia weight and search step, respectively. The notations $X_{\max}$ and $X_{\min}$ are the upper and lower bounds of the search space. Since the algorithm, during the stage, needs to explore a vast space rapidly, the update paradigm and parameters are defined for this stage separately. In Equation (3.3), the notation $step$ is updated by the formula

$$step = \frac{u}{|v|^{(1/\alpha)}}, \tag{3.4}$$

where $\alpha = 0.8$, and u and v are random values in [0,1].

In the second phase of the algorithm, $\omega_1 > A_2$, it is crucial to direct the particles toward the correct direction for an effective search, ensuring that the update paradigm enhances the quality of candidate solutions. Consequently, in this stage, we utilize the guidance of the globally optimal individuals within the particle swarm to drive the particle swarm updates. The update formula is as follows:

$$\begin{cases} V_{i,G+1} = d_1 \cdot \omega_1 \cdot c \cdot r \cdot \left(\left(X_{gbest,G} - X_{i,G}\right)\right) \\ X_{i,G+1} = X_{i,G} + V_{i,G+1} \end{cases}, \tag{3.5}$$

where the symbol r is a random value in [0,1], $c = 2$, and $d_1 \in \{-1, 1\}$.

If $r < 0.6$ and $\omega_1 < A_2$, the particle swarm concludes the exploration of the search space, identifying promising individuals. Our objective is to concentrate the algorithm's search in the vicinity of these individuals to enhance the precision and accuracy of the search results. However, this phase often leads the algorithm into local optima. To address this challenge, this paper integrates the principles of quasi-opposition-based learning [60]. By combining the linear inertia weight with novel guidance positions, this paper proposes a new update paradigm, given in Equation (3.6). Our aim is to enable the algorithm to break free from local optima and enhance the search precision.

$$\begin{cases} V_{i,G+1} = d_2 \cdot c \cdot r \cdot \left(\left((X_{\max} + X_{\min})/2 \cdot \omega_2 - X_{i,G}\right)\right) \\ X_{i,G+1} = X_{i,G} + V_{i,G+1} \end{cases}, \tag{3.6}$$

where the parameter d_2's update formula is as follows:

$$d_2 = \exp\left(-\left(f\left(X_{m_{gbest,G}}\right) \Big/ f\left(X_{f_{i,G}}\right) + \varepsilon\right)\right), \tag{3.7}$$

where $X_{m_{gbest,G}}$ is the best individual in one subpopulation, and ε represents a very small positive quantity. Meanwhile, the finesses of individuals is denoted by $f(X)$, and the another subpopulation is presented as X_f. The two subpopulations will be updated simultaneously using parameters calculated from different individuals within each subpopulation.

In the ultimate phase of candidate solution updates, the update paradigm closely resembles the preceding stage, incorporating a distinct control parameter d_3 . At this stage, $r > 0.6$ and $\omega_1 < A_2$. The introduction of varied control parameters ensures that the search velocity of the particle swarm undergoes continuous changes across different search phases. This strategic utilization of diverse control parameters aims to enable the algorithm to break free from local optima, thereby enhancing the search precision. The update paradigm is as follows:

$$\begin{cases} V_{i,G+1} = d_3 \cdot c \cdot r \cdot \left(\left(\left(X_{\max} + X_{\min}\right)/2 \cdot \omega_2 - X_{i,G}\right)\right) \\ X_{i,G+1} = X_{i,G} + V_{i,G+1} \end{cases}, \tag{3.8}$$

$$d_3 = \exp\left(-\left(f\left(X_{m_{i,G}}\right) \Big/ f\left(X_{f_{i,G}}\right) + \varepsilon\right)\right). \tag{3.9}$$

3.3. Introducing the immigrant operator

To enhance the selection of high-quality individuals and improve the population's quality, inferior individuals were removed from the two subpopulations. Additionally, an immigration operator was used to facilitate information exchange between the subpopulations, thereby enhancing the search accuracy and maintaining a balance between exploration and exploitation. The equation for the immigration operator is as follows:

$$X_{m_{worse,G}} = X_{f_{best,G}}, \tag{3.10}$$

$$X_{f_{worse,G}} = X_{m_{best,G}}, \tag{3.11}$$

which represent worse individual in one of the subpopulations and the best individual in another subpopulation, respectively. The pseudocode of our algorithm is also presented in Algorithm 1.

4. Experimental results and analysis

In this subsection, we provide a detailed analysis of our APSO algorithm. All experiments were conducted on MATLAB 2018b version on a personal computer with an Intel(R) Core(TM) i5-8300H CPU @ 2.30GHz processor and Microsoft Windows 10 Enterprise 64-bit operating system.

For this, 92 benchmarks including a test suite of 23 classic benchmarks, and the CEC2013, CEC2017, and CEC2022 test suites were utilized to verify our algorithm. Among the 92 benchmarks, 29 benchmarks are from CEC2017, 28 benchmarks are from CEC2013, and 12 benchmarks from CEC2022. The maximum number of function evaluations in the algorithm is set to 500. The statistics, including the Wilcoxon's rank-sum test, are calculated from the results of 30 runs. The algorithm was applied in the optimal configuration and optimal scheduling of the ESS, resulting in cost reduction, stabilization of wind power, and decreased wind power grid connection risks.

4.1. Optimization accuracy

In the first group comparison, two PSO variants and three nature-inspired optimization algorithms are taken, namely the MPSO algorithm and the CLPSO algorithm, the SO, the whale optimization algorithm (WOA) [61], and the dragonfly algorithm (DA) [62]. The MPSO, CLPSO and SO are closely related with our proposed algorithm. To ensure that the range of algorithms used for comparative experiments is broad enough, two well-known natural heuristic optimization algorithms were included.

The MPSO and CLPSO represent state-of-the-art PSO variants that address the fundamental limitations of canonical PSO through chaotic inertia weights and comprehensive learning strategies, respectively. Their inclusion provides a direct performance benchmark within the PSO family and allows for a focused comparison of our adaptive mechanisms against established improvement approaches.

The SO is selected as a representative of recent biologically inspired metaheuristics that use sophisticated adaptive phase-switching mechanisms. Unlike PSO-based algorithms, the SO mimics snakes' behavior with distinct exploration and exploitation phases controlled by environmental factors. This selection is particularly valuable because the SO's dynamic stage-based search strategy provides an excellent reference for evaluating our proposed APSO, which also uses phase-dependent update paradigms, albeit through fundamentally different mathematical formulations.

The WOA and DA are included to ensure benchmark diversity across different metaheuristic families. The WOA mimics the bubble-net hunting behavior of humpback whales, while the DA is inspired by dragonflies' swarming behaviors. Their distinct search mechanisms provide a robust testbed to evaluate our algorithm's performance against fundamentally different optimization philosophies, thereby strengthening the generalizability of our findings.

Their parameter settings are the defaults ones recommended by the authors and shown in Table 2, and the experiment on CEC2022 as conducted with dim=10. The overall performance of all results from the 30 runs was evaluated via Wilcoxon's signed rank-sum test with a significant level of $\alpha = 0.05$; the symbols "+", "-", and "=" are used to denote "better", "worse", and "similar" performance, respectively.

Table 3 presents the summary of all comparisons using Wilcoxon's signed rank-sum test for each of the algorithms versus our APSO algorithm with the four test suites containing 92 benchmarks. From Table 3, we can see that our algorithm shows an improvement in performance in 65 out of 92 cases in comparison with the DA, and in 66, 82, 32, and 87 out of 92 cases, respectively, in comparison with the WOA, SO, MPSO, and CLPSO.

Table 2. The settings for all compared algorithms.

Algorithm	Parameter settings
DA	$s = 0.05$, $a = 0.06$, $c = 0.1$, $e = 0.1$, $w = 0.8$, $f = 0.5$
WOA	$a \in [2, 0]$, $A = [-a, a]$, $C \in [0, 2]$, $p \in [0, 1]$, $l \in [-1, 1]$
SO	$Threshold_1 = 0.25$, $Threshold_2 = 0.6$, $c_1 = 0.5$, $c_2 = 0.05$, $c_3 = 2$
MPSO	$\omega \in [0.4, 0.9]$, $c_1 = c_2 = 2$
CLPSO	$\omega \in [0.4, 0.9]$, $c_1 = c_2 = 2$
APSO	$c = 2$, $A_1 = 0.25$, $A_2 = 0.6$

Table 3. The Wilcoxon test results of the comparison experiment in all benchmarks.

	The given algorithms versus APSO				
Test suite:	**23 benchmarks**	**CEC2013**	**CEC2017**	**CEC2022**	**All**
(+/-/=)					Σ
DA	(2/20/1)	(5/14/9)	(2/22/5)	(0/9/3)	(9/65/18)
WOA	(3/15/5)	(1/17/10)	(0/23/6)	(0/11/1)	(4/66/22)
SO	(2/14/7)	(0/27/1)	(0/29/0)	(0/12/0)	(2/82/8)
MPSO	(3/19/1)	(19/4/5)	(16/7/6)	(5/2/5)	(43/32/17)
CLPSO	(2/21/0)	(1/26/1)	(0/28/1)	(0/12/0)	(3/87/2)

4.2. Convergence analysis

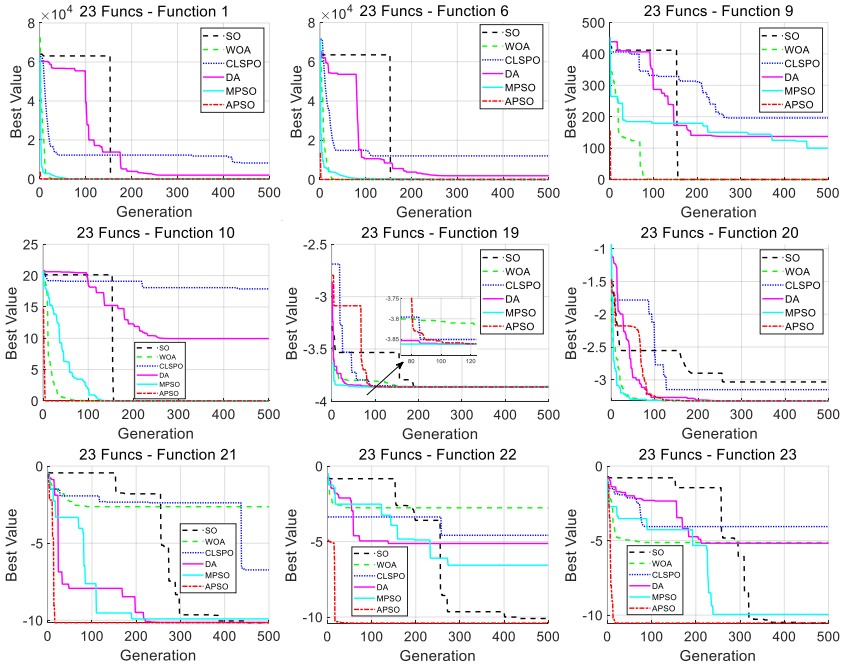

Figure 4. The convergence curves of the algorithms over selected benchmarks of the 23-benchmark test suite.

The proposed APSO algorithm is evaluated from the perspective of convergence speed. For this, 31 benchmarks are randomly selected from different types in four different test suites, and the associated trajectory of the global best over the course of the iteration is depicted as the convergence curve, shown in Figure 4, Figure 5, and Figure 6. From the convergence curve in Figure 4, representing 9 benchmarks randomly selected from 23 classic benchmarks, the convergence curves shows that our algorithm achieves better or similar performance compared with other PSO variants and optimization algorithms on all benchmarks. According to the convergence curve in Figure 5, corresponding to nine benchmarks randomly selected from the CEC2013 test suite, our algorithm achieves better or similar performance compared with the SO for F2, F5, F12, F15, F16, F21, F22, and F26; the WOA for F12, F15, F16, F22, and F26; the CLPSO in F2, F5, F12, F15, F16, F21, and F26; the DA in F2, F5, F15, F16, F21, F22, and

F26; and the MPSO in F15, F16, and F26. In Figure 6, nine benchmarks were randomly selected from the CEC2017 test suite, where our algorithm shows better or similar performance compared with the SO on all selected benchmarks; the WOA on F1, F7, F16, F17, F20, and F28; the CLPSO on F1, F7, F8, F16, F20, F25, F28, and F30; the DA on F1, F17, F20, F28, and F30; and the MPSO on F17, F28, and F30.

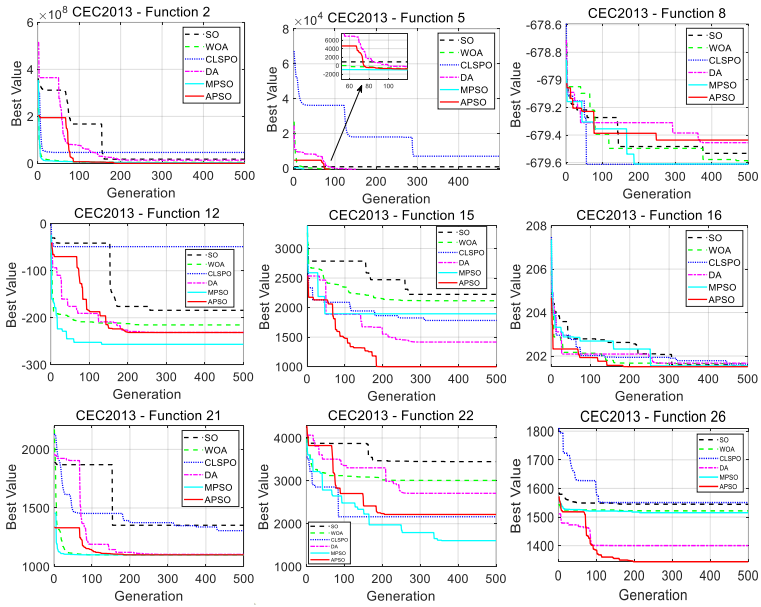

Figure 5. The convergence curves of the algorithms over selected benchmarks of the CEC2013 test suite.

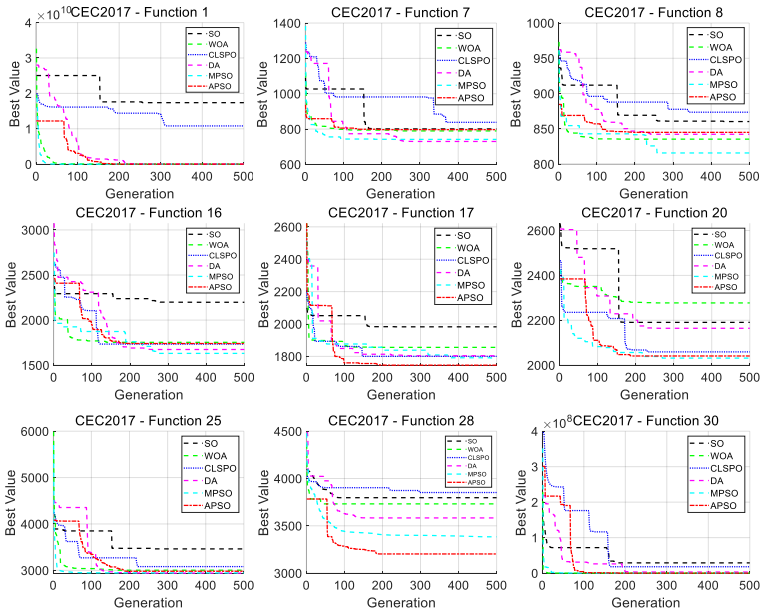

Figure 6. The convergence curves of the algorithms over selected benchmarks of the CEC2017 test suite.

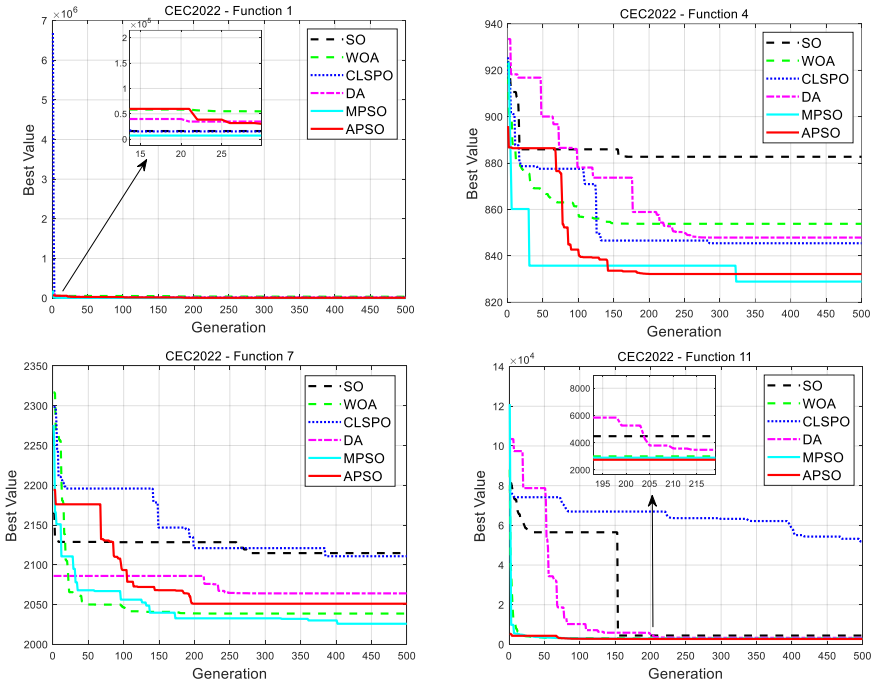

Figure 7. The convergence curves of the algorithms over selected benchmarks of the CEC2022 test suite.

In Figure 7, four benchmarks were randomly selected from the CEC2022 test suite, where our algorithm shows better or similar performance compared with the SO on F4, F7, and F11; the WOA on F1, F4, and F11; than CLPSO on F4, F7, and F11; the DA on F4, F7, and F11; and the MPSO on F11.

Table 4. The benchmarks on which our algorithm obtains better or similar performance.

	Benchmarks on which our algorithm obtains better or similar performance			
Algorithm/test suite	**23 benchmarks**	**CEC2013**	**CEC2017**	**CEC2022**
SO	All the selected functions.	f2, f5, f12, f15-16, f21-22, f26.	All the selected functions.	f4, f7, f11.
WOA	All the selected functions.	f12, f15-16, f22, f26.	f1, f7, f16-17, f20, f28.	f1, f4, f11.
CLPSO	All the selected functions.	f2, f5, f12, f15-16, f21, f26.	f1, f7-8, f16, f20, f25, f28, f30.	f4, f7, f11.
DA	All the selected functions.	f2, f5, f15-16, f21-22, f26.	f1, f17, f20, f28, f30.	f4, f7, f11.
MPSO	All the selected functions.	f15-16, f26.	f17, f28, f30.	f11.

This paper summarizes these results in Table 4 for better readability. It is evident that the proposed APSO algorithm remains competitive with other well-known PSO variants and nature-inspired optimization algorithms.

4.3. Optimal configuration of the ESS for mitigating wind power fluctuations

In this subsection, our APSO algorithm is applied to optimize the configuration of the ESS, in which the energy storage capacity and charge–discharge power were used as the decision variables. The optimization study of the configuration of the ESS was conducted using the wind power output data from a 50-MW wind farm in the year 2020, sampled at hourly intervals. The parameters of the ESS model are presented in Table 5, and the settings for our algorithm are provided in Table 2.

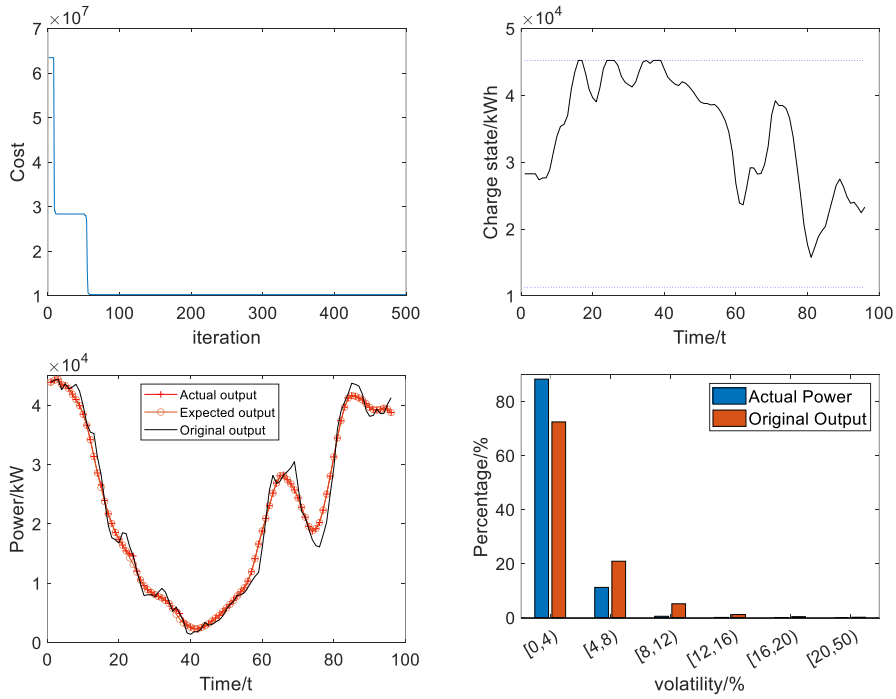

Figure 8. The experimental results of the APSO applied to the model of the optimal configuration of the ESS.

As shown in Figure 8, notable optimization results for the ESS are observed: After 50 generations of optimization, the cost of the ESS has been minimized. The final cost is 1,0281,943 yuan. At this time, the energy storage power and energy storage capacity are 8324 kW and 56,524 kWh, respectively. Furthermore, the smoothed wind power output of the ESS closely aligns with the expected wind power output compared with the original output. At this time, the maximum fluctuation amount is 9.48 MW and the maximum fluctuation rate is 0.1896. The percentage of volatility in the range of [4, 16] has decreased by nearly 20%, whereas the percentage of volatility in the range of [0, 4] has increased by close to 20%. It can also be seen from the charge state that most of the time, the ESS is kept in a relatively stable state during operation, and there is no critical charge and discharge state.

This experiment tests the smoothing effect of the model of the ESS combined with our proposed algorithm, and shows that the proposed APSO algorithm can optimize the configuration of the ESS well, so that the ESS can effectively stabilize wind power while keeping the cost low.

It is important to note that the ESS model used in this study does not account for practical factors such as battery capacity degradation over time, which could impact the long-term performance and economic viability of the ESS. Battery degradation can occur through repeated charge and discharge cycles, leading to a gradual reduction in the storage capacity and efficiency of the system. This degradation could potentially alter the optimal configuration found in this study, affecting both the cost and the effectiveness of the ESS in stabilizing wind power fluctuations.

Future work could incorporate a more realistic battery degradation model, which would consider factors such as the depth of discharge, the cycling life, and the operational conditions over time. By doing so, we would better understand the long-term performance of the ESS and refine the configuration to ensure more accurate and sustainable operation over the entire lifespan of the system.

Table 5. The parameter values of the model of the optimal configuration of the ESS.

Parameters	Values
Unit power cost	1500
Unit capacity cost	1200
Charge–discharge efficiency	0.8
Range of SOC	[0.2,0.8]
Discount rate	0.05

4.4. Optimal scheduling of the ESS with a two-stage scheduling strategy

A simulation example of two-stage scheduling model of an ESS was established in MATLAB. The wind power output of a 25-MW wind farm in China in 2020 and 2021 was used as input data with sampled at interval of 15 min. The previous year was the training data of the prediction model, and the next year was the actual test data of planning energy storage scheduling. The algorithm's parameters and some parameters of the ESS are consistent with Table 2 and Table 5.

To assess the effectiveness of the two-stage scheduling strategy, this paper compares it with several different strategies, including peak–valley arbitrage, the conventional control strategy, and a strategy without ESSs.

Peak–valley arbitrage is a common strategy used in ESSs to take advantage of electricity price fluctuations throughout the day. In this strategy, the ESS charges during periods of low electricity prices (valley periods) and discharges during high electricity price periods (peak periods). The primary goal is to maximize the economic benefit by storing energy when prices are low and selling it when prices are high. This strategy helps balance supply and demand while reducing the overall cost of electricity consumption.

The conventional control strategy typically refers to a rule-based approach where the ESS operates according to predefined conditions or thresholds without adapting to real-time changes in wind power output or electricity prices. For example, it might involve discharging when the wind power generation is low and charging when wind power generation exceeds the demand, but it does not consider market conditions or energy price signals. This approach is simpler but less efficient than more advanced strategies like two-stage scheduling.

This strategy represents the scenario where no ESS is involved in managing wind power fluctuations. In this case, the grid must directly handle the variability of wind power generation, and any excess wind power might be curtailed or wasted when generation exceeds demand. Similarly, when wind generation is insufficient, additional power must be drawn from conventional generation sources, which may not be optimal in terms of cost or environmental impact. This scenario serves as a baseline to compare the performance of ESS-based strategies.

The experimental results, as shown in Figure 9, indicate that the ESS with the two-stage scheduling strategy achieves the lowest expected wind power loss and the highest wind power utilization rate. However, the costs are higher, and the revenue from selling and purchasing electricity is lower.

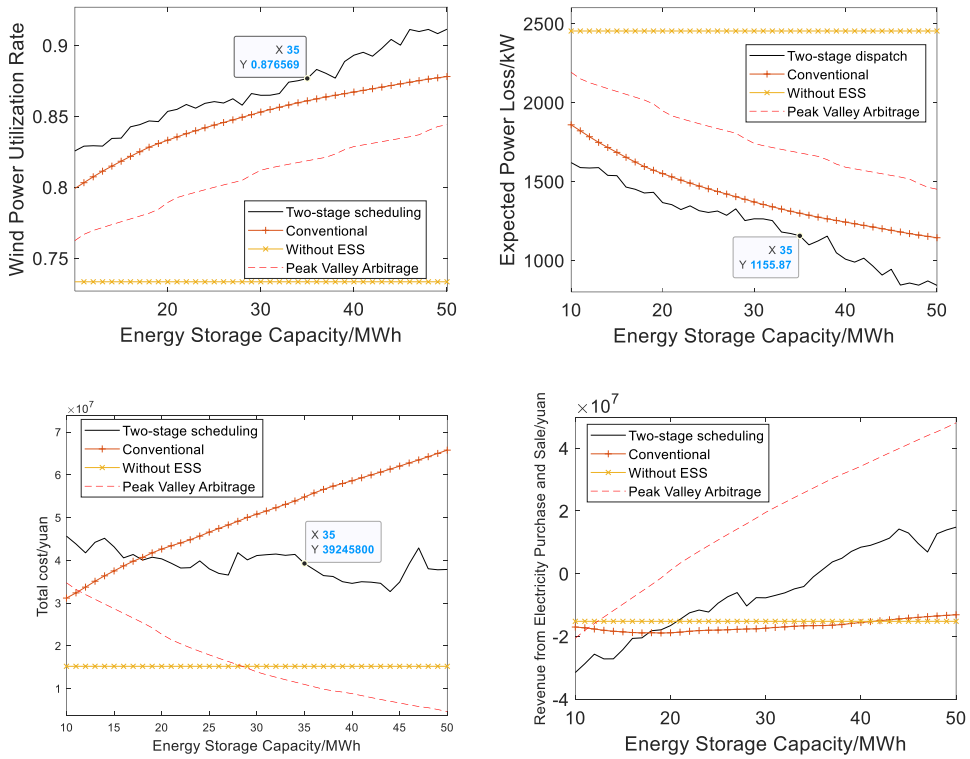

Figure 9. The performance of different strategies that control the ESS.

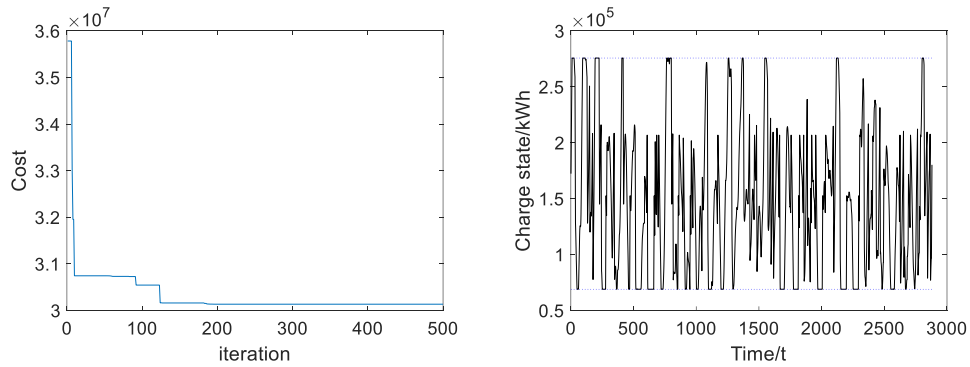

Figure 10. The experimental results of the APSO applied in the model for optimal scheduling of the ESS.

Subsequently, the proposed APSO algorithm was applied to the ESS model, setting the charge–discharge power and energy storage capacity as the decision variables, resulting in the experimental outcomes shown in Figure 10 and Table 6. The results demonstrate a significant reduction of about 9 million yuan in the optimized ESS costs. The optimized ESS costs have been reduced by approximately 23%. Simultaneously, at the same energy storage capacity, the expected wind power loss decreases by 55 kW, resulting in a 4.72% reduction in wind power loss, and the wind power utilization rate improves.

Figure 10 shows that the total cost changes with the number of iterations. The optimal power value of the ESS is 26,121.80 kW, the energy storage capacity is 344,599.59 kWh, and the total cost is 3,0133,094.79 yuan. The expected power loss is 1110.73 kW; the wind power utilization rate is 0.88. The figure also shows that the state of energy storage charge is around 50% most of the time, indicating that the scheduling strategy can effectively extend the life of energy storage.

This experiment tests the performance of the optimal scheduling model of the ESS with the two-stage scheduling strategy combined with our proposed APSO algorithm, and shows that the proposed algorithm can optimize the configuration of the ESS well, so that the ESS can effectively stabilize the wind power while keeping the cost low.

Table 6. The experimental results of the proposed PSO variant applied to the model for optimal scheduling of the ESS.

Performance metric	Result
Energy storage capacity	344599.59 kWh
Total cost	30133094.79 yuan
Expected power loss	1110.73 kW
Wind power utilization rate	0.88

5. Conclusions

This study proposed a novel approach called APSO to address the optimization challenges associated with the configuration of the ESS. Our algorithm introduced several vital contributions. First, a sine function-based linear inertia weight scheme has been devised, dynamically adjusting the inertia weights during different search phases, allowing the algorithm to leverage various update paradigms while maintaining a good balance between exploration and exploitation effectively. Second, the hybrid update paradigm, integrating Levy flight, global best guidance, and quasi-opposition-based learning, enables adaptive strategy switching, enhancing the algorithm's ability to escape local optima. The final contribution involves the incorporation of an efficient dual-subpopulation framework and an immigration operator, enhancing the algorithm's search capabilities and elevating the population quality.

The optimization accuracy and convergence speed were investigated using a test suite containing 92 benchmarks from a test suite of 23 classic benchmarks, and the CEC2013, CEC2017, and CEC2022 suites. Furthermore, this paper used rank-sum test to examine the results of 30 runs for each algorithm. The findings indicate that our proposed algorithm outperforms most compared algorithms, achieving performance improvements in 65, 66, 82, 32, and 87 cases against the DA, WOA, SO, MPSO, and CLPSO, respectively. This confirms the robust optimization accuracy and competitiveness of our proposed method. Finally, we applied the algorithm to the optimization models of ESS configurations. From the results, our algorithm effectively reduced the total cost of the ESS to 10.28 million yuan in the configuration model and reduced the ESS's cost by approximately 23% in the scheduling model. The expected wind power loss decreased by about 4.72%, while determining the optimal storage power (8,324 kW) and capacity (56,524 kWh), smoothing the fluctuations (a maximum fluctuation rate of 0.1896), and reducing the wind power grid connection risks.

While the proposed APSO has shown promising performance in the optimal configuration of the ESS discussed in this paper, there are some areas for further improvement. The algorithm's applicability

to a broader range of real-world engineering problems remains to be explored. The proposed algorithm will be applied to more general engineering problems to address specific real-world challenges in future work.

Author contributions

Chia-Hung Wang: Conceptualization, methodology, supervision, project administration, funding acquisition; Hongzhen Yan: Software, formal analysis, investigation, writing—original draft, visualization; Haitao Liu: Methodology, validation, writing—review and editing; Qigen Zhao: Software, validation, data curation; Xiaojing Wu: Resources, data curation, visualization, validation.

Use of Generative AI tools declaration

The authors declare they have not used artificial intelligence (AI) tools in the creation of this article.

Acknowledgments

This work is partly supported by the Fujian Provincial Department of Science and Technology, China under Grant 2021J011070, and partly by the research fund from Fujian University of Technology under Grant GY-Z18148.

Conflict of interest

All authors declare no conflicts of interest in this paper.

References

1. Y. R. Liu, X. L. Wu, A collaborative optimization approach for configuring energy storage systems and scheduling multi-type electric vehicles using an improved multi-objective particle swarm optimization algorithm, *Processes*, **13** (2025), 1343. https://doi.org/10.3390/pr13051343
2. P. H. A. Barra, W. C. Carvalho, T. S. Menezes, R. A. S. Fernandes, D. V. Coury, A review on wind power smoothing using high-power energy storage systems, *Renew. Sustain. Energy Rev.*, **137** (2021), 110455. https://doi.org/10.1016/j.rser.2020.110455
3. B. Fan, T. Wu, Y. Zhuang, J. Peng, K. Huang, The development of energy storage in china: policy evolution and public attitude, *Front. Energy Res.*, **9** (2021), 797478. https://doi.org/10.3389/fenrg.2021.797478
4. M. A. Hannan, S. B. Wali, P. J. Ker, M. S. A. Rahman, M. Mansor, V. K. Ramachandaramurthy, et al., Battery energy-storage system: A review of technologies, optimization objectives, constraints, approaches, and outstanding issues, *J. Energy Storage*, **42** (2021), 103023. https://doi.org/10.1016/j.est.2021.103023
5. L. Pontes, T. Costa, A. Souza, N. Dantas, A. Vasconcelos, G. Rissi, et al., Operational data analysis of a battery energy storage system to support wind energy generation, *Energies*, **16** (2023), 1468. https://doi.org/10.3390/en16031468

6. S. Hu, H. Yang, S. L. Ding, Z. Tian, B. Guo, H. B. Chen, et al., Model simulation and multi-objective capacity optimization of wind power coupled hybrid energy storage system, *Energy*, **319** (2025), 134887. https://doi.org/10.1016/j.energy.2025.134887
7. C. H. Wang, H. P. Luh, Analysis of bandwidth allocation on end-to-end qos networks under budget control, *Comput. Math. Appl.*, **62** (2011), 419–439. https://doi.org/10.1016/j.camwa.2011.05.024
8. L. E. Anyanwu, A. F. Ogunsina, Q. F. Ohiri, I. Onyewuchi, Renewable energy transition and challenges: solar and wind energy systems optimization through battery storage technology and grid integration strategies, *World J. Adv. Res. Rev.*, **28** (2025), 1938–1952. https://doi.org/10.30574/wjarr.2025.28.3.4226
9. E. Villa-Ávila, D. Ochoa-Correa, P. Arévalo, Advancements in power converter technologies for integrated energy storage systems: Optimizing renewable energy storage and grid integration, *Processes*, **13** (2025), 1819. https://doi.org/10.3390/pr13061819
10. C. H. Wang, K. Hu, X. J. Wu, Multi-robot path planning in online dynamic obstacle environments based on parallel cooperative strategy optimization algorithm, *Discov. Comput.*, **28** (2025), 1–24. https://doi.org/10.1007/s10791-025-09664-5
11. X. Y. Liu, T. Y. Zhu, Z. H. Wei, S. S. Cai, R. Long, Z. C. Liu, Performance analysis of a novel solar-to-hydrogen system with energy storage via machine learning and particle swarm optimization, *Energy*, **315** (2025), 134380. https://doi.org/10.1016/j.energy.2025.134380
12. M. Ding, J. Wu, A novel control strategy of hybrid energy storage system for wind power smoothing, *Electr. Power Compon. Syst.*, **45** (2017), 1265–1274. https://doi.org/10.1080/15325008.2017.1346004
13. T. T. Guo, Y. B. Liu, J. B. Zhao, Y. W. Zhu, J. Y. Liu, A dynamic wavelet-based robust wind power smoothing approach using hybrid energy storage system, *Int. J. Electr. Power Energy Syst.*, **116** (2020), 105579. https://doi.org/10.1016/j.ijepes.2019.105579
14. L. L. Li, Q. Shen, M. L. Tseng, S. Luo, Power system hybrid dynamic economic emission dispatch with wind energy based on improved sailfish algorithm, *J. Clean. Prod.*, **316** (2021), 128318. https://doi.org/10.1016/j.jclepro.2021.128318
15. C. H. Wang, C. J. Lee, X. J. Wu, A coverage-based location approach and performance evaluation for the deployment of 5g base stations, *IEEE Access*, **8** (2020), 123320–123333. https://doi.org/10.1109/ACCESS.2020.3006733
16. C. H. Wang, S. M. Chen, Q. G. Zhao, Y. F. Suo, An efficient end-to-end obstacle avoidance path planning algorithm for intelligent vehicles based on improved whale optimization algorithm, *Mathematics*, **11** (2023), 1800. https://doi.org/10.3390/math11081800
17. H. Shareef, A. A. Ibrahim, A. H. Mutlag, Lightning search algorithm, *Appl. Soft Comput.*, **36** (2015), 315–333. https://doi.org/10.1016/j.asoc.2015.07.028
18. K. C. Divya, P. S. N. Rao, Models for wind turbine generating systems and their application in load flow studies, *Electr. Power Syst. Res.*, **76** (2006), 844–856. https://doi.org/10.1016/j.epsr.2005.10.012

19. N. Kumarappan, R. Arulraj, Multiple installation of dg and dstatcom in radial distribution network using lightning search algorithm, *Proc. Int. Conf. Power, Energy, Control Transm. Syst.*, 2018, 264–269. https://doi.org/10.1109/ICPECTS.2018.8521620

20. F. Firdouse, M. S. Reddy, *A hybrid energy storage system using ga and pso for an islanded microgrid applications,* Energy Storage, **5** (2023), e460. https://doi.org/10.1002/est2.460

21. J. Kennedy, R. Eberhart, Particle swarm optimization, *IEEE Int. Conf. Neural Netw.*, **4** (1995), 1942–1948. https://doi.org/10.1109/ICNN.1995.488968

22. A. G. Gad, Particle swarm optimization algorithm and its applications: a systematic review, *Arch. Comput. Methods Eng.*, **29** (2022), 2531–2561. https://doi.org/10.1007/s11831-021-09694-4

23. J. J. Liang, A. K. Qin, P. N. Suganthan, S. Baskar, Comprehensive learning particle swarm optimizer for global optimization of multimodal functions, *IEEE Trans. Evol. Comput.*, **10** (2006), 281–295. https://doi.org/10.1109/TEVC.2005.857610

24. M. Nasir, S. Das, D. Maity, S. Sengupta, U. Halder, P. N. Suganthan, A dynamic neighborhood learning based particle swarm optimizer for global numerical optimization, *Inf. Sci.*, **209** (2012), 16–36. https://doi.org/10.1016/j.ins.2012.04.028

25. N. Y. Zeng, Z. D. Wang, W. B. Liu, H. Zhang, K. Hone, X. H. Liu, A dynamic neighborhood-based switching particle swarm optimization algorithm, *IEEE Trans. Cybern.*, **52** (2020), 9290–9301. https://doi.org/10.1109/TCYB.2020.3029748

26. L. Y. Wang, L. H. Hong, H. X. Fu, Z. L. Cai, Y. W. Zhong, L. J. Wang, Adaptive distance-based multi-objective particle swarm optimization algorithm with simple position update, *Swarm Evol. Comput.*, **94** (2025), 101890. https://doi.org/10.1016/j.swevo.2025.101890

27. C. H. Wang, K. Hu, X. Wu, Y. Ou, Rethinking metaheuristics: Unveiling the myth of "novelty" in metaheuristic algorithms, *Mathematics*, **13**, (2025), 2158. https://doi.org/10.3390/math13132158

28. Y. Shi, R. Eberhart, A modified particle swarm optimizer, *IEEE Int. Conf. Evol. Comput.*, 1998, 69–73. https://doi.org/10.1109/ICEC.1998.699146

29. M. Taherkhani, R. Safabakhsh, A novel stability-based adaptive inertia weight for particle swarm optimization, *Appl. Soft Comput.*, **38** (2016), 281–295. https://doi.org/10.1016/j.asoc.2015.10.004

30. H. Liu, X. W. Zhang, L. P. Tu, A modified particle swarm optimization using adaptive strategy, *Expert Syst. Appl.*, **152** (2020), 113353. https://doi.org/10.1016/j.eswa.2020.113353

31. Z. Y. Meng, Y. X. Zhong, G. J. Mao, Y. Liang, Pso-sono: A novel pso variant for single-objective numerical optimization, *Inf. Sci.*, **586** (2022), 176–191. https://doi.org/10.1016/j.ins.2021.11.076

32. H. Abouobaida, S. Ullah, A. S. Alsafran, A. Harrison, G. Hafeez, B. Alghamdi, et al., A three-level inverter-based model predictive control design for optimal wind energy systems, *IEEE Access*, https://doi.org/10.1109/ACCESS.2025.3547996

33. H. F. Li, D. J. Wang, M. C. Zhou, Y. S. Fan, Y. Q. Xia, Multi-swarm co-evolution based hybrid intelligent optimization for bi-objective multi-workflow scheduling in the cloud, *IEEE Trans. Parallel Distrib. Syst.*, **33** (2021), 2183–2197. https://doi.org/10.1109/TPDS.2021.3122428

34. W. F. Song, G. Ma, Y. X. Zhao, W. K. Li, Y. X. Meng, Multi-objective reactive power optimization of a distribution network based on improved quantum-behaved particle swarm optimization, *Recent Adv. Electr. Electron. Eng.*, **17** (2024), 698–711. https://doi.org/10.2174/0123520965262291230927052452

35. X. Yao, Y. Liu, G. M. Lin, Evolutionary programming made faster, *IEEE Trans. Evol. Comput.*, **3** (1999), 82–102. https://doi.org/10.1109/4235.771163

36. J. J. Liang, B. Y. Qu, P. N. Suganthan, A. G. Hernández-Díaz, Problem definitions and evaluation criteria for the cec 2013 special session on real-parameter optimization, 2013. Available from: https://www.researchgate.net/publication/256995189.

37. G. Wu, R. Mallipeddi, P. N. Suganthan, Problem definitions and evaluation criteria for the cec 2017 competition on constrained real-parameter optimization, 2017. Available from: https://www.researchgate.net/profile/Guohua-Wu-5/publication/317228117.

38. M. Abdel-Basset, D. El-Shahat, M. Jameel, M. Abouhawwash, Young's double-slit experiment optimizer: A novel metaheuristic optimization algorithm for global and constraint optimization problems, *Comput. Methods Appl. Mech. Eng.*, **403** (2023), 115652. https://doi.org/10.1016/j.cma.2022.115652

39. F. A. Hashim, A. G. Hussien, Snake optimizer: A novel meta-heuristic optimization algorithm, *Knowl.-Based Syst.*, **242** (2022), 108320. https://doi.org/10.1016/j.knosys.2022.108320

40. Y. Q. Yang, S. Bremner, C. Menictas, M. Kay, Battery energy storage system size determination in renewable energy systems: A review, *Renew. Sustain. Energy Rev.*, **91** (2018), 109–125. https://doi.org/10.1016/j.rser.2018.03.047

41. P. A. Dratsas, G. N. Psarros, S. A. Papathanassiou, Battery energy storage contribution to system adequacy, *Energies*, **14** (2021), 5146. https://doi.org/10.3390/en14165146

42. S. L. Wang, Q. Dang, Z. Q. Gao, B. W. Li, C. Fernandez, F. Blaabjerg, An innovative square root-untraced kalman filtering strategy with full-parameter online identification for state of power evaluation of lithium-ion batteries, *J. Energy Storage*, **104** (2024), 114555. https://doi.org/10.1016/j.est.2024.114555

43. S. L. Wang, H. Gao, P. Takyi-Aninakwa, J. M. Guerrero, C. Fernandez, Q. Huang, Improved multiple feature-electrochemical thermal coupling modeling of lithium-ion batteries at low-temperature with real-time coefficient correction, *Prot. Control Mod. Power Syst.*, **9** (2024), 157–173. https://doi.org/10.23919/PCMP.2023.000257

44. S. L. Wang, S. J. Zhang, S. F. Wen, C. Fernandez, An accurate state-of-charge estimation of lithium-ion batteries based on improved particle swarm optimization-adaptive square root cubature kalman filter, *J. Power Sources*, **624** (2024), 235594. https://doi.org/10.1016/j.jpowsour.2024.235594

45. Y. Wei, C. H. Wang, Y. F. Suo, Q. G. Zhao, J. C. Yuan, S. M. Chen, FHO-based hybrid neural networks for short-term load forecasting in economic dispatch of power systems, *J. Netw. Intell.*, **10** (2025), 262–284.

46. E. Rahmani, S. Mohammadi, M. Zadehbagheri, M. Kiani, Probabilistic reliability management of energy storage systems in connected/islanding microgrids with renewable energy, *Electr. Power Syst. Res.*, **214** (2023), 108891. https://doi.org/10.1016/j.epsr.2022.108891

47. Y. M. Chen, J. Peng, G. J. Meng, W. Yao, T. T. Li, Optimal capacity configuration of hybrid energy storage system considering smoothing wind power fluctuations and economy, *IEEE Access*, **10** (2022), 101229–101236. https://doi.org/10.1109/ACCESS.2022.3205021

48. L. Lin, Y. Q. Jia, M. H. Ma, X. Jin, L. Y. Zhu, H. Luo, Long-term stable operation control method of dual-battery energy storage system for smoothing wind power fluctuations, *Int. J. Electr. Power Energy Syst.*, **129** (2021), 106878. https://doi.org/10.1016/j.ijepes.2021.106878

49. X. Y. Wang, M. Yue, E. Muljadi, W. Z. Gao, Probabilistic approach for power capacity specification of wind energy storage systems, *IEEE Trans. Ind. Appl.*, **50** (2013), 1215–1224. https://doi.org/10.1109/TIA.2013.2272753

50. Q. Y. Jiang, H. S. Hong, Wavelet-based capacity configuration and coordinated control of hybrid energy storage system for smoothing out wind power fluctuations, *IEEE Trans. Power Syst.*, **28** (2012), 1363–1372. https://doi.org/10.1109/TPWRS.2012.2212252

51. S. Teleke, M. E. Baran, S. Bhattacharya, A. Q. Huang, Optimal control of battery energy storage for wind farm dispatching, *IEEE Trans. Energy Convers.*, **25** (2010), 787–794. https://doi.org/10.1109/TEC.2010.2041550

52. X. Li, Fuzzy adaptive kalman filter for wind power output smoothing with battery energy storage system, *IET Renew. Power Gener.*, **6** (2012), 340–347. https://doi.org/10.1049/iet-rpg.2011.0177

53. C. Amzallag, J. P. Gerey, J. L. Robert, J. Bahuaud, Standardization of the rainflow counting method for fatigue analysis, *Int. J. Fatigue*, **16** (1994), 287–293. https://doi.org/10.1016/0142-1123(94)90343-3

54. H. Bindner, T. Cronin, P. Lundsager, J. F. Manwell, U. Abdulwahid, I. Baring-Gould, *Lifetime modelling of lead acid batteries*, Forskningscenter Risoe, 2005.

55. C. H. Wang, Q. G. Zhao, R. Tian, Short-term wind power prediction based on a hybrid markov-based pso-bp neural network, *Energies*, **16** (2023), 4282. https://doi.org/10.3390/en16114282

56. H. T. Liu, C. H. Wang, Seams: A surrogate-assisted evolutionary algorithm with metric-based dynamic strategy for expensive multi-objective optimization, *Expert Syst. Appl.*, **265** (2025), 126050. https://doi.org/10.1016/j.eswa.2024.126050

57. K. Hu, C. H. Wang, Parameter identification of solar photovoltaic cell model based on an enhanced swarm intelligence optimization with adaptive parameter tuning and alternating strategies, *Arabian J. Sci. Eng.*, 2025. https://doi.org/10.1007/s13369-025-10663-3

58. T. T. Nguyen, Y. Zeng, C. H. Wang, J. Yuan, T. K. Dao, A solution to the job shop scheduling problem based on an enhanced slime mould algorithm, *Int. J. Comput. Sci. Math.*, **21** (2025), 289–302. https://doi.org/10.1504/IJCSM.2025.148202

59. H. Sharma, J. C. Bansal, K. V. Arya, X. S. Yang, Lévy flight artificial bee colony algorithm, *Int. J. Syst. Sci.*, **47** (2016), 2652–2670. https://doi.org/10.1080/00207721.2015.1010748

60. S. Rahnamayan, H. R. Tizhoosh, M. M. A. Salama, Quasi-oppositional differential evolution, *IEEE Congr. Evol. Comput.*, 2007, 2229–2236. https://doi.org/10.1109/CEC.2007.4424748

61. S. Mirjalili, A. Lewis, The whale optimization algorithm, *Adv. Eng. Software*, **95** (2016), 51–67. https://doi.org/10.1016/j.advengsoft.2016.01.008

62. S. Mirjalili, Dragonfly algorithm: a new meta-heuristic optimization technique for solving single-objective, discrete, and multi-objective problems, *Neural Comput. Appl.*, **27** (2016), 1053–1073. https://doi.org/10.1007/s00521-015-1920-1

AIMS Press